



Alternating direction of catholyte forced flow-through 3D-electrodes improves start-up time in microbial electrosynthesis at applied high current density

Sanne M. de Smit^{a,b}, Jelle J.H. Langedijk^a, Johannes H. Bitter^b, David P.B.T.B. Strik^{a,*}

^a Environmental Technology, Wageningen University and Research, Bornse Weilanden 9, Wageningen 6708 WG, Netherlands

^b Biobased Chemistry and Technology, Wageningen University and Research, Bornse Weilanden 9, Wageningen 6708 WG, Netherlands

ARTICLE INFO

Keywords:

Microbial electrosynthesis
Carbon dioxide utilisation
Biocatalysis
Local conditions
Chain elongation
Mass-transfer

ABSTRACT

Microbial electrosynthesis is an uprising concept for the combined carbon dioxide reduction and electricity storage in the form of green chemical compounds. Although several proof of principle studies show great promise, mass-transfer limitations of substrates, protons and products remains one of the issues that needs to be addressed to bring the systems towards greater scale applications. A previously tested solution formed force flow-through catholyte recirculation, but this set-up encountered difficulties with gas accumulation during start-up at higher current densities ($\sim -10 \text{ kA/m}^3$), creating the need for a bypass to release gas. In this study, start-up at high current density was achieved without a bypass by using an alternating flow-through regime. This regime decreased the operating energy input from 221 to 136 kWh per kg of produced hydrogen and reached acetate production within 10 days after start-up at high current density and elongation to *n*-caproate after 45 days. Mass-transfer studies were included by microsensor measurements of local conditions (hydrogen concentration, pH) combined with thermodynamic calculations at the start and end of 60-days biotic experiments. The microorganisms on the cathode decreased pH gradients and consumed the formed hydrogen. The presence of *Clostridium sensu stricto* 12 and *Peptococcaceae* species were related to chain elongation activity, and the presence of *Methanobrevibacter* was linked to methanogenesis activity. By identifying the effects of different flow-through strategies on local concentrations and functional microbial groups, this work provides insights on the optimal conditions for microbial CO₂ conversion and highlight the application potential of microbial electrosynthesis.

1. Introduction

Microbial electrosynthesis (MES) is a promising technique for the storage of electrical energy in chemical compounds. Basic bioelectrochemical systems typically consist of two electrodes, separated by a membrane. On the anode, an oxidation reaction provides electrons, which gain energy by an applied potential and are then used in reduction reactions on the cathode. The reduction reaction on the cathode is typically catalyzed by a microbial catalyst. The integration of microbial and electrochemical catalysis allows for the electricity-driven formation of multi-carbon compounds from waste streams, such as CO₂. Bioelectrochemical CO₂ conversion, also called electro-fermentation, has yielded various products such as methane, alcohols, proteins and fatty acids[1–5]. Although these proofs of concept are promising, several steps need to be taken to understand how electro-fermentations systems

could be best designed and scaled-up. An important focus point to work towards upscaling is the improvement of substrate and electron availability for the microorganisms on the cathode[1]. By incorporating microorganisms on the cathode, a biofilm is formed, to which electrons can be supplied, directly or indirectly via e.g. hydrogen formation. The growth and productivity of the biofilm depends on its access to substrate and electrons and the removal of products[6]. A dense biofilm (>400 μm) facilitates high electron uptake rates and improved biocatalytic performance[7,8], but inevitably also leads to mass-transfer limitations. Therefore, pH and hydrogen gradients are likely to occur, resulting in different local conditions at the electrode surface when compared to the bulk conditions[9–13]. The pH gradients affect the microbial community selection and thermodynamic limitations, as well as substrate and electron donor availability[14,15].

To diminish the effects of significant local gradients of pH,

* Corresponding author at: Environmental Technology, Wageningen University and Research, Bornse Weilanden 9, 6708 WG Wageningen, Netherlands.

E-mail addresses: harry.bitter@wur.nl (J.H. Bitter), david.strik@wur.nl (D.P.B.T.B. Strik).

<https://doi.org/10.1016/j.cej.2023.142599>

Received 25 January 2023; Received in revised form 27 February 2023; Accepted 22 March 2023

Available online 25 March 2023

1385-8947/© 2023 The Author(s). Published by Elsevier B.V. This is an open access article under the CC BY license (<http://creativecommons.org/licenses/by/4.0/>).

substrates, products or energy (like hydrogen), mass-transfer can be improved by changing the flow-regime[16]. Previously, 3-dimensional flow-through electrodes have been demonstrated as a solution for better mixing of the anodic or cathodic chamber[17,18]. Although these flow-through configurations worked well for previous systems, problems were encountered when starting the flow-through configured systems at high current density (i.e. systems operating on at least -10 kA/m^3). Starting bio-electrochemical CO_2 elongation systems at high current density stimulates microbial activity[19], but also leads to local accumulation of excess hydrogen gas between the membrane and low-porous electrode. This hydrogen gas accumulation hinders the contact between the electrolyte in the cathode compartment (catholyte), the membrane, and the electrode, which introduces for example high electrolyte resistances[20]. As a temporary solution, a bypass was used to release accumulated gaseous hydrogen via an extra catholyte recirculation outflow port, but catholyte could also flow through the bypass [21]. About 50% of the recirculation flowed alongside the cathode through the bypass instead of through the cathode. As a consequence of this measure, about 50% of the nutrients from the recirculated medium cannot reach the biofilm and the decreased flow velocity through the biofilm can result in mass-transfer limitations. Both the decreased nutrient supply and mass-transfer limitations can negatively affect the cathodic biofilm activity. Therefore, the recirculation flow through the cathode chamber needs to be optimized to allow start-up at high current densities in a way that the mentioned bypass was not required.

In this study, the use of alternating direction of catholyte flows through porous electrodes was assessed to decrease mass transfer issues and the start-up time of microbial electrosynthesis at applied high current densities was improved. The recirculation flow-through was alternated from two sides of the cathode to allow alternate build-up gas removal and hydrogen transfer to the cathode, which removed the need for a bypass. Additionally, local distribution of electrical current, hydrogen concentration and pH at different locations in the cathode was studied with microsensors measurements. The local conditions were used for identification of mass-transfer limitations and local thermodynamic and microbial analysis. The links between local conditions and presence of certain microorganisms give valuable insights about the conditions required for optimization of microbial-electrochemical conversion processes.

2. Materials and methods

2.1. Reactor setup and flow-through configuration

The reactor setup for both the abiotic and biotic experiments was used as described by De Smit, Langedijk, van Haalen, Lin, Bitter and Strik [21]. In short, plexiglass flow-through plates were used for the reactor assembly, with a Ti/Pt-Ir MMO anode (Magneto Special Anodes BV, Netherlands) and a graphite felt cathode (3 mm thick, Rayon Graphite Felt, CTG Carbon GmbH, Germany) with three layers separated by plastic mesh spacers (3 layers mesh between cathode 1 and 2 and 3 layers between cathode 2 and 3). A video instruction of the reactor assembly can be found in [21]. The cathode layers were connected in parallel to a n-stat potentiostat (IVIUM, Netherlands) with titanium wire (0.8 mm thick, grade 2, Salomon's metalen, Netherlands) with 1Ω between each connection and the working electrode plug (Fig. 1). The resistances were added between the cathode layer connection and working electrode plug to allow multimeter (Fluke 175 True RMS Multimeter) measurements of current and potential over these connections without having to break the connection. The anode (30 mL) and cathode (90 mL) compartment were separated by a cation exchange membrane (21.3 cm^2 projected surface area, Fumasep FKS, Fumatech BWT GmbH, Germany). Both anolyte and catholyte were recirculated via a 250 mL recirculation bottle (Fig. 1), with total volumes of respectively 200–300 and ~ 400 mL for the anolyte and catholyte (including tubing). For the first abiotic flow experiment (Fig. 2), a bypass was used as described by De Smit, Langedijk, van Haalen, Lin, Bitter and Strik [21]. For the following experiments, alternating flow-through catholyte recirculation was used. To allow for alternating flow-through, some adaptations were made. Solenoid valves (SMC, type VDW22JA) were installed at four points around the cathode chamber (Fig. 1A – D). The valves were controlled with a relay module (Fieldpoint FP-DO-410). The relay module was controlled with computer software (LabVIEW 2015). The code used in LabVIEW can be found in the Supporting Information (SI Fig. S1). The recirculation was alternated between two directions: either from valve D to valve A or from valve C to valve B (Fig. 1).

Besides the valves, analog potentiometers (Fieldpoint FP-AI-110) were installed to measure the cell potential, current distribution, and the individual cathode potentials. The cathode potentials were measured against the top reference (QM710X, Q-is, Oosterhout,

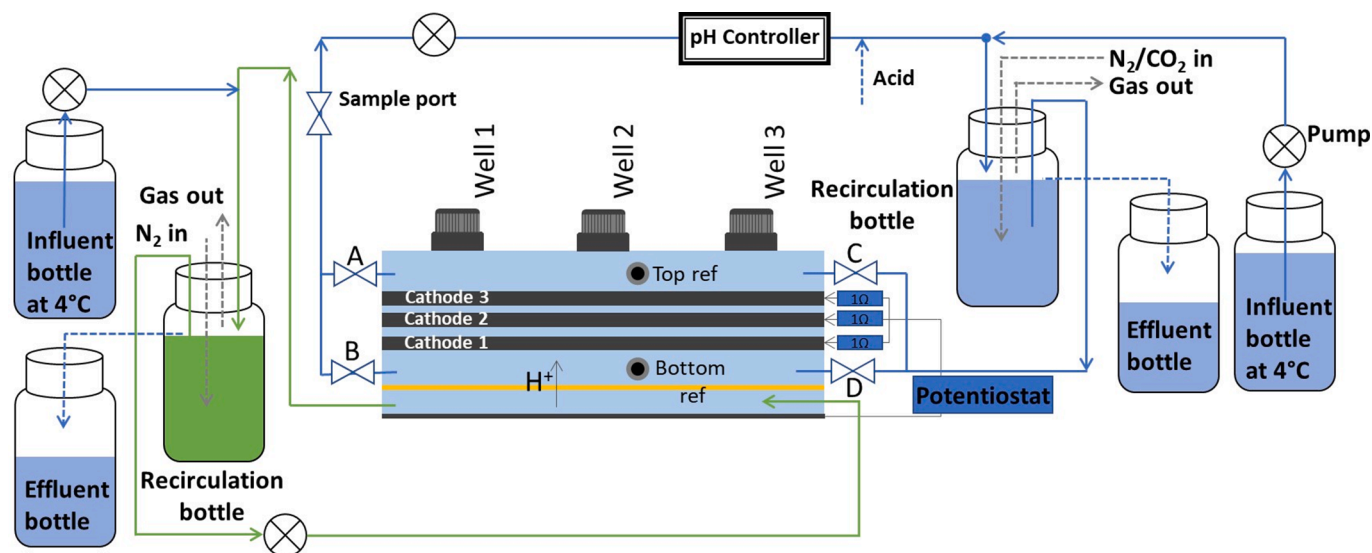


Fig. 1. Schematic reactor setup of electrochemical reactor with switching valves (A-D) used for the alternation of flow-through electrolyte recirculation. The anolyte recirculation is shown in green for viewing purposes. (For interpretation of the references to colour in this figure legend, the reader is referred to the web version of this article.)

Netherlands) (Fig. 1) and not corrected for the electrolyte resistance. However, for the calculations, the cathode potential of cathode 3 was used for all three cathode layers, since it was demonstrated that the electric field potential offset between the top reference and cathode layer 3 was negligible [21].

Regarding the reactor operation, all parameters were set as described by De Smit, Langedijk, van Haalen, Lin, Bitter and Strik [21]: temperature 30 °C, flow rate of catholyte and anolyte recirculation 10 L/h, –200 mA from anode to cathode, 100 LN/h CO₂ and 233.3 LN/h N₂ purging in catholyte recirculation bottle, N₂ purging in anolyte recirculation bottle. The pH was measured (QMP108X, Q-is, Oosterhout, the Netherlands) in the catholyte recirculation and controlled (Ontwikkelwerkplaats, Elektronica ATV, the Netherlands) at 5.8 with the addition of 1 M HCl. The reactor media compositions changed slightly with the switch from abiotic to biotic experiments. The abiotic catholyte composition was the same as described by de Smit, Buisman, Bitter and Strik [22], while the abiotic anolyte consisted of 7.5 g/L Na₂HPO₄·2H₂O, 3.0 g/L KH₂PO₄, 0.05 g/L MgSO₄·7H₂O, 0.01 g/L Ca(OH)₂. For the biotic experiments, ammonium was added to the electrolytes (0.2 g/L NH₄Cl and 0.18 g/L (NH₄)₂CO₃ respectively in the catholyte and anolyte). The biotic catholyte also contained 3.23 g/L (98%) sodium 2-bromoethanesulfonate. The anolyte and catholyte media were added at flow rates corresponding with hydraulic retention times of respectively 4 and 14 days from bottles stored in a fridge (4 °C flushed with gaseous N₂). The biotic reactors were inoculated with 10 vol% fresh inoculum from a biomass growth reactor, acclimatized with comparable conditions; fed with gaseous CO₂, operated at –200 mA to graphite felt electrode (7.7 kA/m³), bulk pH 5.8, temperature 30 °C; which showed production of fatty acids (C2-C4). The inoculation moments were day 5 and day 10.

2.2. Analyses

The volatile fatty acid and alcohol concentrations in the recirculation catholyte were measured three times a week during the biotic experiments. For this, 2 mL catholyte was sampled from the reactor and stored in the freezer until analysis. Analysis was performed 1–2 times per week. On the day of the analysis, the samples were centrifuged at 10 000 rpm for 10 min. Next, the sample was diluted 10 or 20 times to a total volume of 1,5 mL, depending on the concentrations of VFAs. 1,35 mL diluted sample was mixed with 0,15 mL 15% formic acid to acidify the sample. 1 µL was injected with an autosampler in a gas chromatograph with a flame ionization detector (GC-FID) (Agilent 7890B). The FID detects alcohols (Methanol to hexanol) and VFA's (C2-C8).

From day 40 of the biotic phase, the off-gas was measured three times per week. No off-gas measurements were performed from day 0–40 because no methane formation was expected due to the 2-bromoethanesulfonate presence in the medium and catholyte. Since the flow-through was alternated, it was expected that the hydrogen off-gas concentration might fluctuate with the fluctuating flow. To measure a representative, average hydrogen fraction in the off-gas, off-gas was collected in a 10L gas bag (Calibrated instruments, Inc.) for 30 min. The nitrogen and carbon dioxide concentrations were analysed on a GC-TCDD (Shimadzu GC-2010), and the hydrogen concentration was analysed on a GC with a thermal conductivity detector (TCD) (Agilent HP 6890 GC). Methane was analysed on a GC with a pulse discharge detector (PDD) (Global Analyzer Solutions CompactGC).

2.3. Microsensor analyses

During both abiotic and biotic experiments, microsensor measurements (with LS18 laboratory stand, MM3-2 micro-manipulator, MC-232 Motor Controller of Unisense A/S, Denmark) were used to measure local pH (pH-50, Unisense A/S, Denmark) and hydrogen (H₂-50, Unisense A/S, Denmark) concentrations. The method was applied as described by De Smit, Langedijk, van Haalen, Lin, Bitter and Strik [21]. The abiotic

profile measurements were made in reactors that were stabilized for at least 60 h. Important to mention is that during biotic operation, the graphite felt cathode was never pierced by the microsensor to prevent changes of the flow-through path. The graphite felt cathode was only pierced on day 60 of the experiment, during the measurements of the hydrogen and pH profiles at the end of the biotic phase. Electric Potential (EP-100, Unisense A/S, Denmark) measurements revealed that the local electric field potential was affected by the alternating flow-through operation. Therefore, the EP correction method described by De Smit, Langedijk, van Haalen, Lin, Bitter and Strik [21] was not applicable. To obtain reliable pH logging values, the pH microsensor tip was placed near the fixed reference electrodes (3 M KCl Ag/AgCl, QM710X, Q-is, Oosterhout, Netherlands) (top and bottom, Fig. 1). Measurements with the EP sensor were used to determine the exact location with 0 mV offset between the EP sensor and the fixed reference electrode (both Ag/AgCl electrodes). The pH was logged at exactly those locations to ensure there was no electric field interference of the measurements.

2.4. Microbial community analysis

2.4.1. Samples collection and DNA extraction

The microbial communities at different cathode layers and in the suspension were examined with Next Generation Sequencing. Samples were taken at the end of the 60 day biotic operation, stored at –20 °C, and DNA was extracted with the Powersoil DNA isolation kit (Qiagen, USA) according to the instruction manual. The DNA concentration and purity were measured with a NanoDrop spectrophotometer (Thermo Fisher Scientific, Germany).

2.4.2. Sequencing of 16S rRNA genes and bioinformatics

The isolated DNA was amplified with PCR, targeting the 16S V3 and V4 region with gene-specific sequences selected from Klindworth, Pruesse, Schweer, Peplies, Quast, Horn and Glöckner [23]. Illumina adapter overhang nucleotide sequences were added to the gene-specific sequences, resulting in the full length primers (with standard IUPAC nucleotide nomenclature) shown in SI Table S1.

For the index PCR, Nextera UD indexes set D was used. After the rDNA sequencing data was acquired, the reads were joined, de-noised and quality filtered with the dada2 tool. For the taxonomic analysis, the sequences were classified with the tool feature-classifier, with a pre-trained Naive Bayes classifier trained on the amplicon of primer set 341F and 805R, extracted from SILVA v. 132 reference database [24]. Diversity analyses were performed with the qiime2 diversity tool. This bioinformatics process was performed on 4 October 2022. For the results of this study, the most significant operational taxonomic units (OTUs) were presented for each sample, with a cut-off value of 3% relative abundance. Microbiota raw sequencing data are submitted to the ENA database (<https://www.ebi.ac.uk/ena>) under accession number PRJEB55694.

2.4.3. Scanning electron microscopy imaging

From the cathode layers, Scanning Electron Microscope pictures were taken to visualize the biomass distribution. Samples of cathode (~50 mm²) were stored at 4 °C in biotic catholyte and fixed with 2.5% glutaraldehyde for ~4 months at 4 °C. Prior to dehydration, the samples were rinsed three times by replacing the liquid with demi water. For the dehydration, the liquid was replaced by graded ethanol solutions (10, 30, 50, 70, 80, 90, 96, and twice 100%) for 10 min each. The samples were dried with critical point drying (Leica EM CPD-030, Leica Microsystems, Germany) with CO₂. The samples were attached on the SEM stubs with carbon glue (Leit-C Conductive Carbon Cement, van Loenen Instruments, the Netherlands) and coated with tungsten sputter coating (12.0 nm, from two sides with 45° angle, Leica SCD 500, Austria) to finalize the preparation for the imaging. The SEM images were obtained with a Magellan 400 SEM (FEI Company, Hillsboro, OR, USA) at an

acceleration voltage 2 kV and beam current of 13 pA at RT.

2.4.4. Calculations

For the calculations described below, all units are shown in square brackets within the formulas. To calculate the power demand per kg produced hydrogen (in kWh/kg H₂), the cell potential (V_{cell} in V or J/C) was used (measured between the anode and the cathode connection before the parallel split), Faraday constant 96485.33 C/mol, 100% electron recovery into hydrogen:

$$96485.33 \left[\frac{C}{mol_{e^-}} \right] * 2 \left[\frac{mol_{e^-}}{mol_{H_2}} \right] * \frac{1[h]}{3600[s]} * \frac{1[mol_{H_2}]}{2.016 * 10^{-3} [kg_{H_2}]} * V_{cell} \left[\frac{J}{C} \right] * 10^{-3} \left[\frac{kW}{W} \right] = Power \left[\frac{kWh}{kg_{H_2}} \right] \quad (1)$$

To calculate the cathode layer resistance (in Ωm²), Eq. (2) was used:

$$Resistance [\Omega m^2] = \frac{Cathodelayerpotential[V] * projectedsurfacearea[m^2]}{Cathodelayercurrent[A]} \quad (2)$$

The electron recovery into volatile fatty acids (η_{VFA}) and hydrogen (η_{H₂}) was calculated based on the measured concentrations of volatile fatty acids in the liquid phase at the sampling time Conc_{VFA,t}, the measured current in mA (i.e. mC/s) at the sampling time (Current_t), the catholyte outflow rate at the sampling time (Q_t, calculated based on the inflow rate and acid addition over time):

$$\eta_{VFAs} = \frac{96485 \left[\frac{mC}{mmol_{e^-}} \right] * Conc_{VFA,t} \left[\frac{mmol}{L} \right] * Q_t \left[\frac{L}{h} \right] * X \left[\frac{mmol_{e^-}}{mmol_{VFA}} \right]}{Current_t \left[\frac{mC}{s} \right] * 3600 \left[\frac{s}{h} \right]} \quad (3)$$

To calculate the electron recovery into hydrogen, the hydrogen flow was calculated based on the hydrogen and nitrogen fractions in the measured off gas (fraction_{offgas}H₂, fraction_{offgas}N₂), the reactor temperature (Temp) and the ideal gas law, assuming that the N₂ was inert inside the reactors:

$$Flow_{H_2} \left[\frac{mmol_{H_2}}{h} \right] = \frac{fraction_{offgas} H_2 [\%] * 233.3 \left[\frac{LN}{d} \right] * 101325 [Pa]}{fraction_{offgas} N_2 [\%] * 24 \left[\frac{h}{d} \right] * 8.314 \left[\frac{J}{K * mol} \right] * Temp [K]} \quad (4)$$

The electron recovery into hydrogen was calculated based on the hydrogen flow and the current measured at the sampling time of the hydrogen:

$$\eta_{H_2} = \frac{96485 \left[\frac{mC}{mmol_{e^-}} \right] * Flow_{H_2} \left[\frac{mmol_{H_2}}{h} \right] * 2 \left[\frac{mmol_{e^-}}{mmol_{H_2}} \right]}{Current_t \left[\frac{mC}{s} \right] * 3600 \left[\frac{s}{h} \right]} * 100 [\%] \quad (5)$$

The electron recovery into methane was also calculated based on the methane fraction in the off-gas, in the same way as the electron recovery into hydrogen, with the adjustment that methane contains 8 mmol e⁻ per mmol methane.

The hydrogen concentration in the catholyte was calculated based on the measured hydrogen fraction in the off-gas (fraction_{offgas} H₂), with a Henry coefficient of 7.7E-06 mol/(m³Pa)[25] and a pressure of 1 atm (101325 Pa).

$$Hydrogenconc [\mu M] = 7.7 * 10^{-6} \left[\frac{mol}{m^3 Pa} \right] * 101325 [Pa] * \frac{fraction_{offgas} H_2 [\%]}{100 [\%]} * 10^3 \left[\frac{\mu mol * m^3}{L * mol} \right] \quad (6)$$

3. Results and discussion

3.1. Increased power demand due to gas build-up at high current density

To demonstrate the issues with the state-of-art flow-through configuration during start-up at high current density, abiotic reactors were started up with controlled current of -10.4 kA/m³. The cell potential was measured to calculate system power demand for production of hydrogen. The previously suggested flow-through recirculation flow was used [17,18] and a bypass outlet of the cathode chamber was placed between the membrane and the cathode (Fig. 2B). When the recirculation flow was forced through the graphite felt cathode (bypass closed), the cell potential increased simultaneously with gas build-up between the membrane and the cathode (Fig. 2, grey planes and SI Fig. S2). To release the build-up gas and lower the system power demand, the bypass was opened (Fig. 2A, white planes). Opening the bypass caused the cell potential to drop almost instantaneously (Fig. 2A, zoom in frame).

The cell potential correlates with the system power input (right y-axis, Eq. (1)), a cell potential increase correlates with a higher power demand. The power needed during the time with the bypass opened (white planes) was 146 kWh/kg hydrogen (assuming 100% CE to hydrogen), while it increased to 221 kWh/kg hydrogen when the bypass was closed (Fig. 2A, right y-axis). Presumably, the high power with the bypass closed can be explained by the gas build-up between the membrane and cathode, which caused increased ionic resistance [20]. To keep the cell potential low, and thus reduce the operation energy costs, the bypass would need to be opened to prevent build-up of gas between the membrane and cathode. However, with the bypass open, about 50% of the flow is directed through the bypass and not through the cathode. This would mean that 50% of the electrolyte entering the cathode chamber leaves the cathode chamber through the bypass, not being forced through the cathode layers. With the flow only partially going through the cathode layers, nutrient supply to the cathode biofilm is limited. To allow both removal of excess gas build-up and flow through the cathode layers, the reactor configuration was adapted to a cross flow-through design: a second cathode inflow point was installed, the bypass was replaced through a second reactor outlet, and all in- and outlets were provided with switchable valves (Fig. 3B).

To measure the power demand of switching between two different flow-through directions, the cell potential was measured over time whilst different flow direction alternation intervals were tested (Fig. 3A). The flow was alternated between *away from the membrane* (orange dashed arrow, Fig. 3B) and *towards the membrane* (green filled arrow, Fig. 3B), with increasing interval time between alternation time (0.5 min to 10 min). Compared to the previous situation with the bypass open, the power demand was lower with alternating flow. The longer the time interval between flow direction alternation (x-axis, Fig. 3A), the more the maximum cell potential increased with local gas accumulation between the membrane and cathode (Fig. 3A, maximum values). With the increasing cell potential, the power demand also increased, leading to a higher average power demand for the experiments with longer time between the flow direction switches. The replicate reactor showed the same trend (SI Fig. S3).

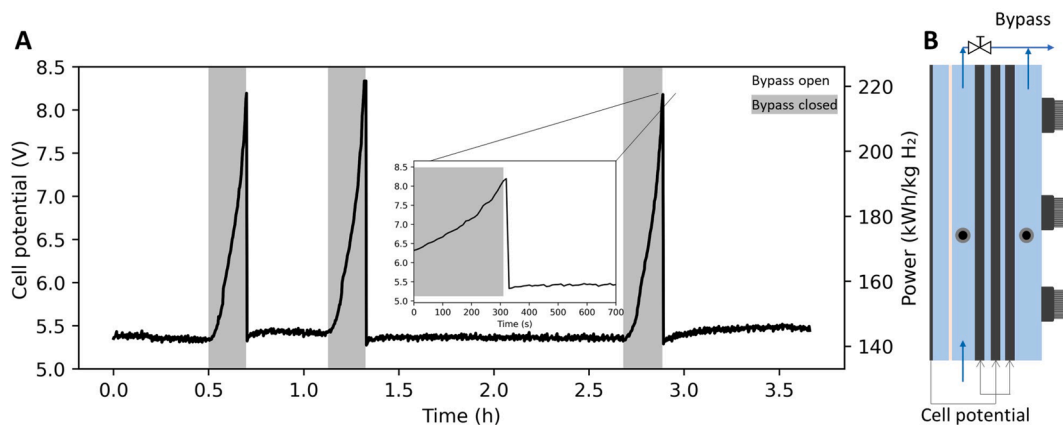


Fig. 2. Cell potential and corresponding power demand over time with -200 mA (-10.4 kA/m³) applied cathode current under abiotic conditions. The bypass was closed three times (grey area) for ± 10 min. Based on the cell potential, the power demand per kg hydrogen was calculated (right y-axis, see M&M for details).

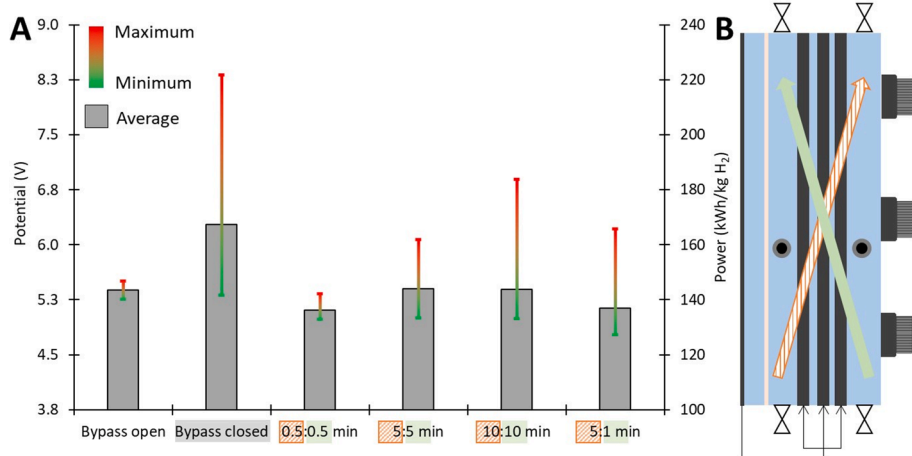


Fig. 3. Electric power demand per kg produced hydrogen (right y-axis) calculated based on the cell potential (left y-axis) averaged over 3.5 h of switching flow direction between away from (orange dashed) and towards (green filled) the membrane of a reactor operated at -10.4 kA/m³ under abiotic conditions. The error bars show the minimum and maximum measured power demand during the 3.5 h. (For interpretation of the references to colour in this figure legend, the reader is referred to the web version of this article.)

3.2. Alternating flow-through allows cathode resistance decrease and refreshing of local pH and hydrogen

Besides the effect of different alternating flow-through intervals on power demand, the mass-transfer to the cathode and the cathodic bio-film is an additional important parameter. To elucidate on the effect of flow-changes on local conditions, and thus mass-transfer to the cathode, several parameters were measured over time: cell potential (A), cathode layer resistances (C) and current densities (D), as well as local pH I and hydrogen concentrations (F) (Fig. 4). To properly show the trends at both flow-through directions over several minutes, these measurements were performed in the reactor with a 5:5 min switching between flow towards (green filled) and flow away from (orange dashed) the membrane.

The cell potential increases with the flow away from the membrane (orange dashed) and remained rather constant (5.0–5.1 V, Fig. 4A) at the minimum value with the flow towards the membrane (green filled). Note that although it seems that the cell potential with the flow towards the membrane is decreasing over time, this was not measured over the whole 25 h course of the experiment. Since the gas build up also increased over time, the increase in cell potential seems a consequence of the gas build-up between the membrane and cathode. Remarkably, the cell potential (Fig. 4A) was the only parameter that linearly increases over time during the flow away from the membrane, while cathode layer current and resistance, local pH, local hydrogen change in a “switch-like” manner, i. e. the values change right at the moment the flow direction switches.

The cathode resistances were higher with the flow towards the

membrane (green filled) compared to the values with flow away from the membrane (orange dashed, Fig. 4C). The resistances corresponded with the current densities, lower resistances resulted in higher (more negative) current densities (Fig. 4D). When comparing the three cathode layers, the cathode layer closest to the membrane (cathode 1) had on average the lowest resistance and the highest current ($\sim 85\%$ of the total current), whereas the furthest cathode layer (3) had the highest resistance and lowest current (Fig. 4C and D). These trends were observed through the whole experiment and are likely related to the distance from the anode, as could be proven by e.g. electrochemical impedance spectroscopy measurements.

The pH measuring spot was chosen on the outer side of the cathode (Fig. 4B) to investigate the effect of switching flow-through direction on the pH dynamics in a possible “dead zone” location where less mixing might occur. The pH was relatively high (7.7) when the flow was away from the membrane (orange dashed, Fig. 4E) and decreased approximately 0.5 pH unit with the flow direction switch to towards the membrane (green filled). The high values with the flow away from the membrane indicate a high local pH at the cathode surface, caused by the proton consumption for hydrogen formation. This local pH is different from the controlled recirculation pH (5.8), showing indeed less mixing in the measured location. During the direct mixing with the recirculation electrolyte (towards the membrane flow), the local pH did not decrease to the pH of the catholyte during the 5 min. The little pH decrease indicates that with recirculation speed of 10 L/h, it takes longer than 5 min to completely mix the 90 mL cathode chamber with the electrolyte.

The two local hydrogen measurements give valuable insights in the

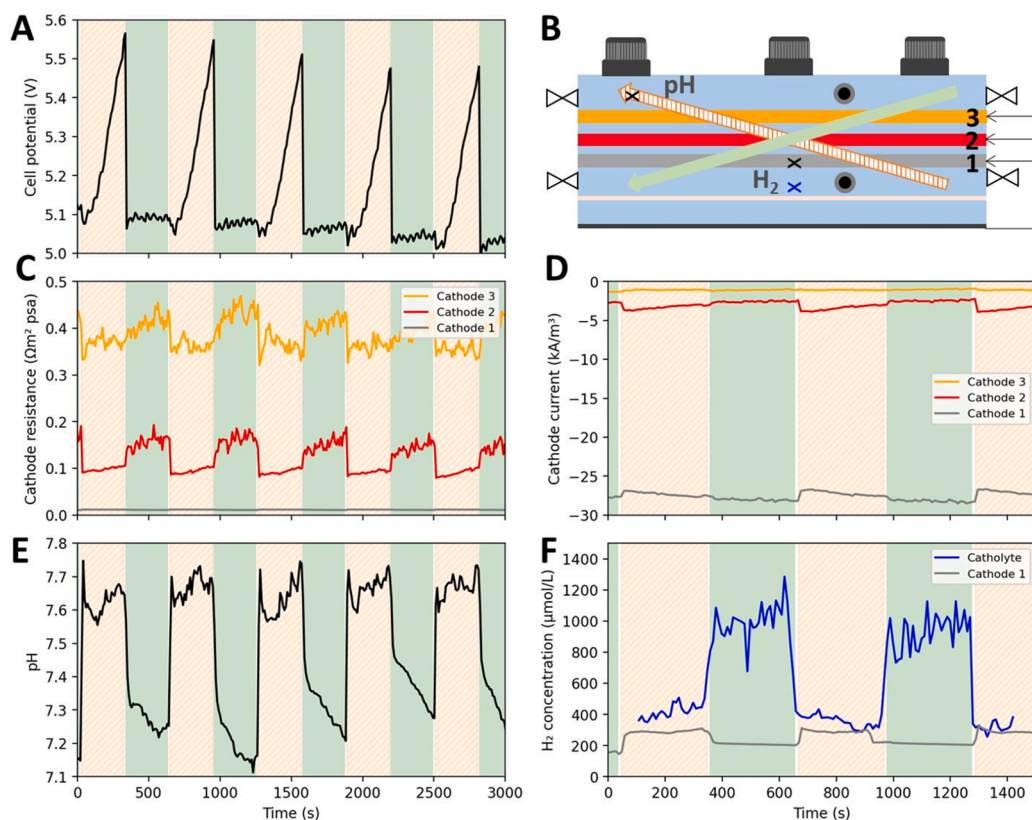


Fig. 4. Cell potential (A), cathode layer resistances (C) and current densities (D), and local pH (E) and local hydrogen concentrations (F) over time during 5:5 min flow switching between flow away from (orange dashed) and towards (green filled) the membrane under abiotic conditions. The locations of the pH and hydrogen measurements are indicated in B. Note: the different hydrogen measurements were overlapped in (F) for viewing purposes. (For interpretation of the references to colour in this figure legend, the reader is referred to the web version of this article.)

dynamics of the hydrogen distribution in the cathode 1 closest to the membrane and the electrolyte between the cathode and the membrane (Fig. 4F). When the flow was directed *towards the membrane* (green plane), the hydrogen concentration inside cathode 1 decreased (grey line). Simultaneously, an increase in the electrolyte next to the membrane was measured (blue line). When the flow was switched from *towards the membrane* to *away from the membrane* (orange dashed plane), the hydrogen concentration in the electrolyte immediately dropped, showing removal of excess built-up hydrogen gas next to the cathode, and an increase in hydrogen concentration inside the cathode was measured. With the flow *away from the membrane*, the hydrogen is brought into cathode 1, while the flow *towards the membrane* relocated the highest local hydrogen concentration from the cathode to the catholyte. This shows a direct reversing effect of the highest hydrogen concentration relocation simultaneous with the reversing of the flow-through direction. Fig. 4F also shows that the concentration of hydrogen in the catholyte was always higher than the concentration of hydrogen in the cathode. This could create an advantage for hydrogen consuming microorganisms in the catholyte over those growing on the cathode. However, from an earlier work with a similar experimental design, it has been reported that CO_2/N_2 sparging in the recirculation bottle constituted for hydrogen loss in the catholyte, meaning that the high hydrogen concentration in the catholyte was mostly lost via the recirculation and thus less available for the biofilm [21].

3.3. Biotic start-up at high current showed faster *n*-butyrate production with alternating flow-through strategy

Based on the previous results in the abiotic reactor, a flow switching interval was considered to both increase the hydrogen concentration in

the cathode and also allow for mixing of the cathode chamber with the recirculated catholyte. To direct the local hydrogen to the cathode layers, the time with flow *towards the membrane* must be kept short, to potentially prevent hydrogen loss and increase the concentration in cathode 1. However, flow *towards the membrane* was required to refresh possible dead zones and decrease the cell potential (and thus energy demand). Thus, for mixing of the liquid in the catholyte chamber (90 mL), 1 min flow *towards the membrane* was chosen based on the theoretical hydraulic retention time of 32.2 sec with recirculation 10 L/h. For the flow *away from the membrane*, 5 min was chosen to allow for hydrogen-rich catholyte recirculation flow availability at the cathode layers for 83.3% of the time of a full cycle. The resulting 5:1 interval for the switch of flow direction led to a lower power demand when compared to switching with equal intervals between both flow directions (Fig. 3). With this chosen flow-through switching strategy, two biotic reactors were started to test the feasibility of start-up at high current density.

The two biotic reactors were operated with the 5:1 strategy for 60 days at a current density of -10 kA/m^2 . The volatile fatty acids in the recirculated catholyte (Fig. 5A and B) and the hydrogen concentration in the off-gas were measured to characterize productivity and electron recovery into products (Fig. 5C and D). Production of acetate was achieved within 7 days after start-up and the first *n*-butyrate was observed on day 13. Lower concentrations of acetate and *n*-butyrate were measured in the second biotic reactor (Fig. 5B). Although the fast start-up of autotrophic acetate production has previously been shown [26], we observed, for the first time, a substantially faster increase in the *n*-butyrate concentration over time. After 40 days, the *n*-butyrate concentration was 26 mM (Fig. 5A), while other comparable studies reported 2 to 10 times lower *n*-butyrate concentrations [27–29] at 40 days

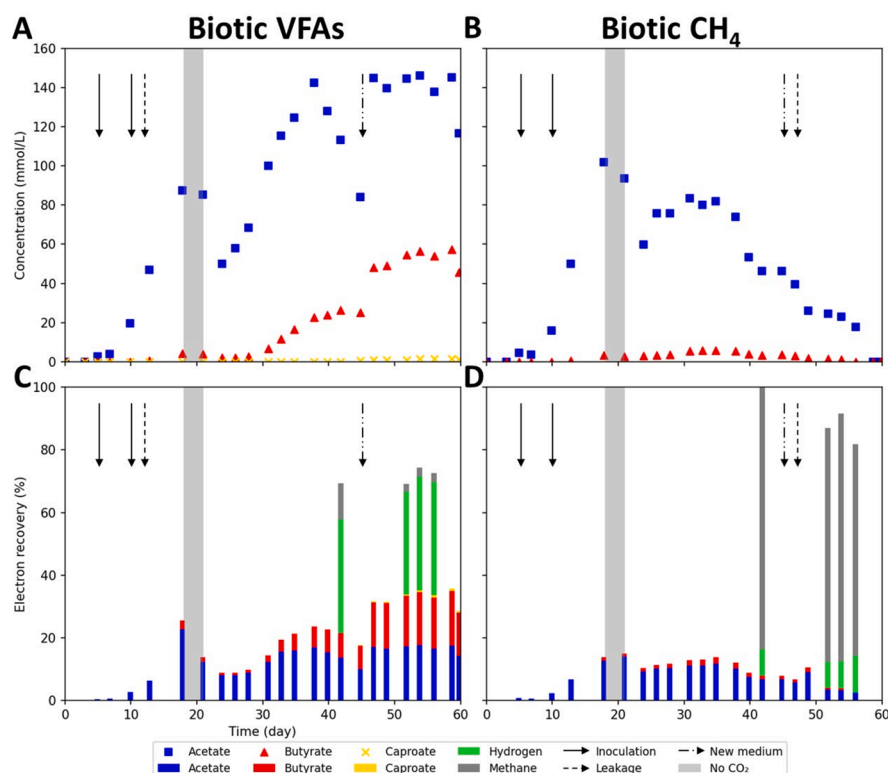


Fig. 5. Concentrations of volatile fatty acids (acetate, *n*-butyrate and *n*-caproate) over time during the biotic experiments, with inoculation moments indicated by filled arrows. Of the two reactors, one showed mainly chain elongation (CE: A,C), while the other showed mainly methanogenesis (CH_4 : B, D). On day 18, the CO_2 supply was cut off for three days (grey plane). On day 45, the medium supply in the fridge was refreshed (dash dot arrow). Leakages are indicated with dashed arrows and always followed by addition of fresh medium to replace the leaked volume. Electron recovery values were calculated as described in the materials and method.

after start-up of microbial electrosynthesis with CO_2 as sole carbon source, with *n*-butyrate formation from earliest 3 days after start up [28]. These studies used 5 A/m^2 [28,29] while the current study applied 92 A/m^2 projected surface area, so suggestively the *n*-butyrate production from acetate was stimulated by the high applied current density in this study.

Besides the concentrations, the electron recoveries were also significantly high, with recoveries reaching up to 60% for the total fatty acid production (Fig. 5C). In the second reactor, methane was measured as the main product (biotic CH_4 , Fig. 5D). The methane was measured at four different timepoints after the acetate and *n*-butyrate dropped in the catholyte. Even though the methane fraction in the outgoing gas was low, the total electron recovery reached up to 100%. To investigate the difference in the electron recovery gap between the methane and volatile fatty acid producing reactors, a sample of anolyte was taken on day 59 and analysed for VFA's. The anolyte of the biotic CH_4 reactor contained 155 mg L^{-1} acetate, and the anolyte of the biotic VFAs reactor contained 885 mg L^{-1} acetate (and 235 mg L^{-1} butyrate). Based on the hydraulic retention time, it was calculated that up to 15% of the electrons ended up as volatile fatty acids in the anolyte in the biotic VFAs reactor, likely contributing to the gaps in the electron balances (Fig. 5C and D). These product losses need to be addressed and prevented when aiming at upscaling. Despite the losses, the results from this study are promising for the use of high current density and the alternating flow-through regime for the fast start-up of carboxylate production from CO_2 .

The methane formation was unexpected because a methanogenesis inhibitor (2-bromoethanesulfanoate, 2-BES) was added to the medium [30]. To verify that the 2-BES was not depleted in the catholyte of the reactors, its concentration was measured in the catholyte of the two reactors and in the medium supply (SI Fig. S4). Although the concentrations in the catholyte were 1.5 times lower than in the medium, 2-BES was still detected in the catholyte, and no difference was observed between the 2-BES concentration in the two different reactors.

The striking difference between the main product of the two biotic reactors could thus not be explained by operating parameters or

differences in the bulk conditions. It is plausible that the difference in results was caused by a difference in the initial attachment of the biomass from the inoculum. For the VFAs reactor, the chain elongating microorganisms could have been attached to a location on the cathode with favourable conditions, whilst for the CH_4 reactor, the methanogens could have been attached to a location on the cathode with favourable conditions. For example, pH values between 5.0 and 6.0 have shown to be more favourable for chain elongation microorganisms [31]. This difference in initial attachment location could have led to advantage for different microbial groups and thus steered the selectivity towards the microbial group with advantageous conditions. Therefore, linking local conditions to the corresponding observed activity could elucidate favourable conditions for either methanogenic or chain elongation microorganisms which is necessary for further scale up.

3.4. Local hydrogen decreased during biotic run while local pH stabilized

To investigate the local conditions for microbial activity, characterization was performed by local microsensor measurements of hydrogen and pH throughout the cathode layers and electrolyte next to the cathode on day 0 and day 60 (Fig. 6). At time 0, the conditions at the cathode layers, inner and outer catholyte differed significantly within the reactors. Depending on the location and the flow direction, measured hydrogen concentrations ranged from ~ 200 to $600 \mu\text{M}$ (Fig. 6A) and the pH ranged from 5.0 to 7.0 (Fig. 6D).

The hydrogen concentration in the catholyte and cathode layers at day 0 showed the same trend as earlier observed in Fig. 4F. Briefly, the highest local hydrogen concentration moved from the catholyte to the inside of the cathode layers when the flow was switched from *towards the membrane* (green filled) to *away from the membrane* (orange dashed) in both reactors (Fig. 6A, SI Fig. S5). The hydrogen concentration was detected (range of 250 to $400 \mu\text{M}$) in all three cathode layers and in the catholyte on the outer side of the cathode when the flow was *away from the membrane*, even though most hydrogen production probably occurred at cathode 1, which had significantly higher current density

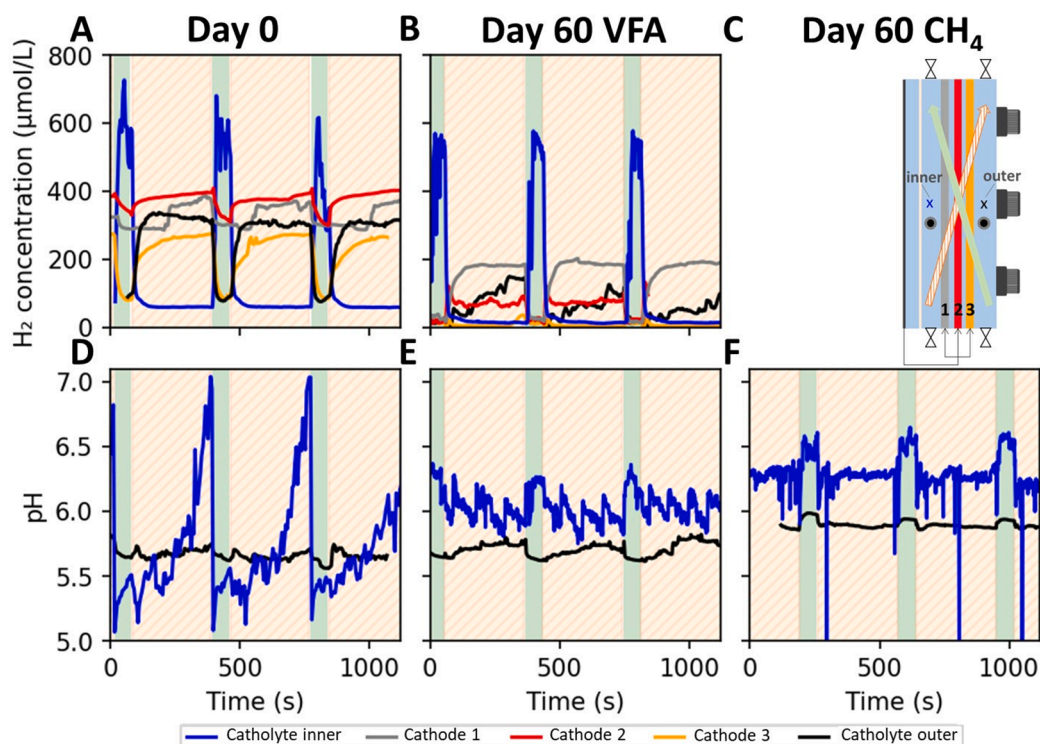


Fig. 6. Local concentrations of hydrogen throughout the cathode layers and the pH in two electrolyte locations before inoculation (A, D), one biotic chain elongating (VFAs) (B, E) and one biotic methane (CH_4) forming (F) system with alternating flow of 5 min away from (orange dashed) and 1 min towards (green filled) the membrane. The times are normalized for viewing purposes. (For interpretation of the references to colour in this figure legend, the reader is referred to the web version of this article.)

(Fig. 4D). The wide range of conditions (H_2 and pH) between different spots supports the hypothesis that the attachment location of the microbial community in the inoculum may lead to the development of different dominant microbial groups.

At the end of the biotic experiments (day 60), the hydrogen concentrations inside the cathode layers and in the catholyte on the outer side of the cathode were lower compared to the concentrations on day 0 (Fig. 6B). The hydrogen concentration profiles measured at the bottom well (lowest sampling point at the bottom of the reactor) were similar to the profiles obtained at the middle well (SI Fig. S7B). However, at the top well, the hydrogen concentration at the cathode layer 1 and 3, and inner and outer catholyte was lower (SI Fig. S7A). The hydrogen concentrations were the highest inside cathode 1, where the highest current densities were measured (SI Fig. S6), whereas little hydrogen was measured inside cathode 3 (Fig. 6B). To also quantify the hydrogen concentration in the bulk catholyte, e.g. the recirculation catholyte, the hydrogen concentration was calculated based on the measured off-gas concentration (Eq. (6)). The hydrogen concentration was $1.8 \mu\text{M}$ in the biotic VFAs reactor and $0.5 \mu\text{M}$ in the biotic CH_4 reactor (day 40–56). These low concentrations are likely caused by stripping of hydrogen by the incoming CO_2/N_2 gasflow in the recirculation. The measured low hydrogen concentrations at the top of cathode layers 1 and 3 were probably caused by removal of hydrogen via the outgoing recirculation liquid. The lower hydrogen concentrations at the end of the biotic experiment compared to day 0 indicate hydrogen consumption by the microbial community growing on the cathode. Due to technical issues, the local hydrogen concentration in the methanogenesis reactor was only measured on the outer side of the cathode (SI Fig. S8). The hydrogen concentration was substantially lower in the methanogenesis reactor (SI Fig. S8) when compared to the chain elongation reactor. This lower hydrogen concentration in the outer catholyte of the methanogenesis reactor was measured over time during the whole biotic run (SI

Fig. S8). The lower hydrogen concentration could be due to higher hydrogen consumption in the methanogenic reactor, which could be caused by higher affinity for hydrogen by methanogenic microbes compared to chain elongation microbes.

The local pH also changed between the start and end of the biotic measurements. On day 0, the pH between the membrane and cathode (inner, Fig. 6D) increased several pH units when the flow was directed away from the membrane (orange dashed). This increase in pH after switching the flow direction to away from the membrane became less evident over time, as the pH remained approximately constant during both flow directions on day 60 (Fig. 6E and F). On the last day of the biotic runs, the pH in the methanogenesis reactor (Fig. 6F) was slightly higher than in the chain elongation reactor (Fig. 6E). The pH on the outer side of the cathode gives valuable insights on the mixing of the systems. It is expected that poor mixing might lead to “dead zones”, and therefore, higher pH, as observed in the abiotic reactor (Fig. 4E). However, on day 60, the pH on the inner side was similar to the outer side pH (5.8–6.3 and 5.8, respectively). This similarity in pH at different locations of the reactor indicates that the one-minute flow towards the membrane (green filled) was a successful strategy to homogenise the catholyte and prevent the accumulation of high pH catholyte.

3.5. Gibbs free energy changes based on local conditions

Based on the local pH and hydrogen concentration measurements, thermodynamic feasibility of different reactions could be determined for the different locations in the reactor. The thermodynamic feasibility can be used as theoretical parameter for determination of productive sites in the biotic reactors. The suggested minimum required Gibbs reaction energy for microbial growth is -20 kJ/reaction [32]. More negative Gibbs reaction energy correspond with higher energy gain for microorganisms and thus better microbial feasibility. To investigate the

Table 1

Local Gibbs free energy of different possible reactions in the CO₂-fed electrochemical reactors before (abiotic) and at the end of the biotic run (biotic), calculated based on the measured local conditions at different locations in the reactor (inner catholyte, cathode 1, cathode 2, cathode 3 and outer catholyte, shown in Fig. 4AB and DE). For undetected hydrogen concentrations in the abiotic reactor, 1 μM was assumed. The values are given for both hydrogen and cathode (at measured cathode potential) as electron donor and coloured based on their magnitude. Compound dissociation and solubility were taken into account for the calculations (details in SI appendix I).

		Day 0					Day 60 (VFAs reactor)				
		Inner	Cat 1	Cat 2	Cat 3	Outer	Inner	Cat 1	Cat 2	Cat 3	Outer
1 Hydrogen formation	$2H^+ + 2e^- \rightarrow H_2$		-113.9	-113.8	-102.8			-98.4	-99.4	-102.8	
2 Acetogenesis	$2CO_2 + 4H_2 \rightarrow CH_3COO^- + H^+ + 2H_2O$	-47.6	-51.1	-51.2	-50.0	-50.7	-31.8	-28.9	-27.0	-20.7	-27.6
	$2CO_2 + 4H_2 \rightarrow CH_3COO^- + H^+ + 2H_2O$	-23.8	-25.6	-25.6	-25.0	-25.3	-15.9	-14.5	-13.5	-10.3	-13.8
			-140.4	-140.3	-140.7			-113.7	-113.9	-114.0	
3 Acetate to n-butyrate elongation	$2CH_3COO^- + 2H_2 + H^+ \rightarrow CH_3(CH_2)_2COO^- + 2H_2O$	-11.1	-8.3	-8.4	-7.4	-7.9	-29.5	-27.2	-26.2	-22.8	-26.5
	$2CH_3COO^- + 2H_2 + H^+ \rightarrow CH_3(CH_2)_2COO^- + 2H_2O$	-11.1	-8.3	-8.4	-7.4	-7.9	-29.5	-27.2	-26.2	-22.8	-26.5
			-122.6	-122.6	-122.6			-126.0	-126.0	-126.0	
4 n-Butyrate to n-caproate elongation	$CH_3COO^- + CH_3(CH_2)_2COO^- + 2H_2 + H^+ \rightarrow CH_3(CH_2)_4COO^- + 2H_2O$	-23.1	-17.5	-17.8	-15.8	-16.8	-67.1	-62.6	-60.4	-53.7	-61.0
	$CH_3COO^- + CH_3(CH_2)_2COO^- + 2H_2 + H^+ \rightarrow CH_3(CH_2)_4COO^- + 2H_2O$	-11.6	-8.8	-8.9	-7.9	-8.4	-33.6	-31.3	-30.2	-26.9	-30.5
			-122.7	-122.7	-122.7			-129.7	-129.7	-129.7	
5 Hydrogenotrophic methanogenesis	$CO_2 + 4H_2 \rightarrow CH_4 + 2H_2O$	-136.6	-130.3	-130.8	-126.8	-128.9	-147.7	-137.1	-132.8	-119.4	-134.0
	$CO_2 + 4H_2 \rightarrow CH_4 + 2H_2O$	-34.2	-32.6	-32.7	-31.7	-32.2	-36.9	-34.3	-33.2	-29.8	-33.5
			-147.0	-147.0	-147.0			-133.1	-133.1	-133.1	
6 Acetoclastic methanogenesis	$CH_3COO^- + H^+ \rightarrow CH_4 + CO_2$	-10.3	-7.0	-7.1	-6.7	-6.9	-21.0	-19.8	-19.7	-19.5	-19.7

feasibility of different microbial conversions, the available Gibbs free energy was calculated in the catholyte and inside the different cathode layers (cathode 1–3) for different possible reactions [33–37] (Table 1). The feasibility was calculated both for hydrogen as electron donor (white filled cells) and for direct electron uptake as energy source (blue filled cells), at day 0 and day 60 of the biotic VFAs reactor. The CH₄ reactor was not considered since no hydrogen data was available for day 60. Based on the thermodynamic calculations, all reactions with CO₂ as substrate (2 and 5, Table 1) show values more negative than –20 kJ/reaction on day 0 in all tested biotic reactor locations. The difference in Gibbs free energy yield between different locations was small – up to 10 %. With the measured cathode potential, direct electron uptake reactions have a more negative Gibbs reaction energy compared to mediated electron uptake (i.e. using hydrogen as an electron donor) (Table 1, kJ/mol 2e⁻ vs kJ/mol hydrogen), as also suggested previously [35]. However, it is unknown whether all the present microorganisms have the capability of direct electron uptake. Since the Gibbs reaction energy values do not differ substantially between different locations, the impact of the different local hydrogen concentrations and pH did not seem to significantly affect the thermodynamic feasibility.

A thermodynamic shift can be observed between the start (day 0) and the end (60 d) of the biotic experiment. At the start, acetogenesis (reaction (2)) and methanogenesis (reaction (5)) were both feasible and competing for the same substrate (CO₂). As shown previously, the competition was won by acetogenesis in the chain elongation reactor, and by the methanogenesis in the methane forming reactor (Fig. 5A and B). On day 0, the Gibbs free energy for methanogenesis was slightly more negative (–30 to –40 kJ/mol hydrogen) than for acetogenesis (–23 to –25 kJ/mol hydrogen), at all locations. This shows a small thermodynamic advantage for methanogenic microorganisms. On day 60, the thermodynamic favourability shifted from acetogenesis towards acetate elongation reactions to butyrate and caproate (reactions (3) and (4)), mainly because of the increased acetate and butyrate concentrations in the reactor. Also acetoclastic methanogenesis was more favourable at day 60 compared to day 0 (reaction (6)). At the end of the biotic phase, the difference in Gibbs free energy between the different locations was slightly higher compared to day 0. In particular at cathode 3, the Gibbs free energy decreased up to 20% (less negative free energies), meaning that all the reactions were energetically less favourable at this position compared to day 0. The differences in thermodynamic feasibility are a direct result of the differences in local conditions,

showing the importance of monitoring local conditions.

3.6. Qualitative visualization of biofilm and identification of microbial communities on the three cathode layers

After showing the thermodynamic feasibility of both chain elongation and methanogenesis during the biotic phase, the position of the biofilms on the cathodes layers was visualized and the species present in the microbial community were identified. The relative amount of biofilm and biofilm structures on the different cathode layers were visualized with Scanning Electron Microscopy (SEM), and the presence of planktonic cells in the catholyte was measured with optical density. The optical density values were 0.146 and 0.067 for the biotic chain elongation reactor and the methane producing reactor, respectively. This indicates a higher presence of suspended microorganisms in the chain elongation reactor, which could be explained by the slightly higher hydrogen concentrations in the catholyte (SI Fig. S8). The Scanning Electron Microscopy showed diversity in the coverage of the graphite felt electrode at the measured spots, corroborating with the different local cathodic current, hydrogen concentration and pH as described above (Fig. 7, overview pictures in SI Figs. S9–S12).

The SEM pictures were taken from the top, middle and bottom of the three different graphite felt cathode layers (Cat 1–3), corresponding with the reactor orientation used in the previous figures (e.g. Fig. 6C). Samples after 60 days were imaged with overview pictures (SI Figs. S9–S11) and with close-up pictures of the biofilm structures (Fig. 7). For the biotic volatile fatty acid producing reactor, most biofilm coverage was seen on the extracted samples from cathode 3 and the top of cathode 1 (SI Fig. S11A, Cat 3 and Cat 1 top), whilst for the biotic methane producing reactor most biofilm coverage was found in the middle and bottom parts of cathode 1 and a bit in the top of cathode 3 (SI Fig. S11B, Cat 1 mid, Cat 1 bottom and Cat 3 top). The cathode pieces with the least biofilm coverage showed biofilm structures on the graphite felt cathode fibres, whilst the cathode pieces with higher biofilm coverage also showed biofilm structures between the fibres (Fig. 7). As opposed to cathode layers 1 and 3, hardly any biofilm structures were observed on cathode 2. The differences in the locations with the highest biofilm coverage between the two biotic reactors could be related to differences in optimal conditions between the chain elongation and methanogenic microorganisms. For example, at cathode 1, the hydrogen production was the highest (Fig. 6A and B) and this cathode showed dense biofilms

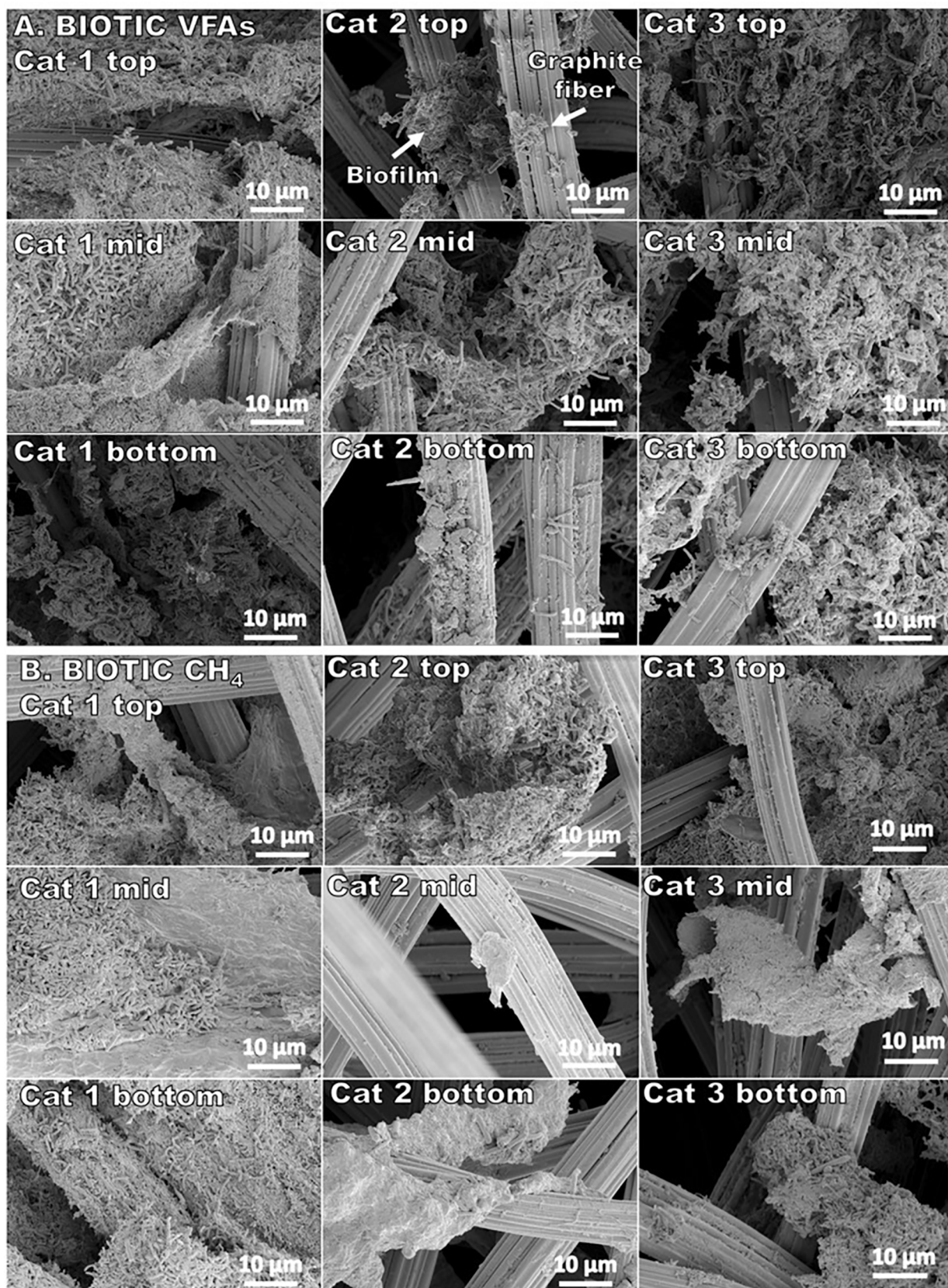


Fig. 7. Detail Scanning Electron Microscope image of biofilm on graphite felt pieces of different reactor locations from the biotic volatile fatty producing reactor (A VFAs, top 9 images) and the biotic methane producing reactor (B CH₄, bottom 9 images), both sampled on day 60. The reactor orientation and the definition of bottom, mid and top is in accordance with the schematic of the reactor shown in Fig. 6C.

Table 2

Relative abundance of different microbial groups found in the biofilm at the different cathode layers (mid) and suspended culture of the biotic reactor with chain elongation (VFAs) and methane formation (CH₄) after 60 days of biotic operation. Only the classified genera with Operational Taxonomic Unit (OTUs) with at least 3% relative abundance are shown in this table.

Affiliation	Biotic VFAs				Biotic CH ₄			
	Catholyte	Cathode 1	Cathode 2	Cathode 3	Catholyte	Cathode 1	Cathode 2	Cathode 3
<i>Clostridium sensu stricto</i> 12	63.1%	41.1%	35.1%	41.0%	0.8%	0.9%	22.8%	0.6%
<i>Peptococcaceae</i>	1.2%	8.1%	27.5%	18.5%	0.3%	15.8%	31.4%	20.0%
<i>Methanobrevibacter</i>	4.6%	18.2%	4.6%	11.1%	12.8%	26.9%	12.4%	23.7%
<i>Bacteroides</i>	4.5%	1.9%	2.4%	2.2%	25.7%	5.5%	2.3%	6.6%
<i>Rhodocyclaceae</i>	1.5%	0.8%	2.0%	1.7%	23.9%	6.4%	2.8%	9.3%
<i>Rikenellaceae U29-B03</i>	8.1%	4.6%	2.2%	2.6%	1.0%	2.2%	1.0%	1.5%
<i>Rikenellaceae RC9 gut group</i>	3.6%	6.9%	7.3%	7.9%	0.6%	6.2%	4.6%	3.4%
<i>Erysipelotrichaceae UCG-004</i>	0.2%	0.3%	0.5%	0.3%	0.8%	6.4%	2.5%	5.0%
<i>Desulfovibrio</i>	0.4%	0.2%	0.1%	0.1%	3.2%	2.2%	0.7%	1.9%
Other (<3%)	12.8%	17.9%	18.4%	14.5%	30.9%	27.5%	19.4%	27.9%

in the CH₄ reactor (Fig. 7B, Cat 1) at two locations (mid and bottom), whilst only for one location (top) in the VFAs reactor (Fig. 7A, Cat 1). Generally, a higher biofilm coverage was observed (by eye) on the cathode parts where the flow-through recirculation was entering the cathode, so the outer sides of the cathodes (SI Fig. S12). The reason for lower biofilm coverage on cathode 2 could be a filtering function of cathode 1 and 3, which were located as the first cathode layers at the flow-through inlet points. As a result, greater flocculant parts of biomass might be forced to adsorb or attach to cathode 1 and 3 rather than passing those cathodes to reach cathode 2.

To identify which microorganisms were accountable for the observed biotic structures, Next Generation Sequencing was performed with samples from the suspension and the three cathode layers. Regions of the 16S rRNA were extracted and classified down to genus level (Table 2).

In the reactor with chain elongation products (acetate, butyrate, and caproate), *Clostridium sensu stricto* 12 related species were the most abundant microorganisms (Table 2, Biotic VFAs). In the methanogenic reactor, *Peptococcaceae* and *Methanobrevibacter* species had the highest relative abundance (Table 2, Biotic CH₄). The *Peptococcaceae* species were abundantly present on the cathodes of both reactors. Other microorganism groups with significant relative abundance are *Bacteroides* and *Rikenellaceae* U29-B03 and RC9 gut group. *Rhodocyclaceae* species were found in the methanogenic reactor, but with substantial lower abundance values in the chain elongation reactor. Interestingly, the *Peptococcaceae* species has low relative abundance in the catholyte and high relative abundance on the cathode, suggesting an affinity to grow attached to the graphite felt. The *Bacteroides* however, shows an opposite trend, suggesting a higher affinity for suspended growth. The presence of certain microorganisms can be linked to the observed products to suggest the role and function of the different microbial and Archaea groups.

Several *Clostridium* species are known for CO₂ fixation and/or elongation of acetate to *n*-butyrate and *n*-caproate[38–47]. It is therefore likely that the *Clostridium sensu stricto* 12 related species were responsible for the production of *n*-butyrate and *n*-caproate (Fig. 5A). Uncultured *Peptococcaceae* have been found with high relative abundance in microbial electrosynthesis systems where CO₂ was reduced to acetate [48] and in a culture producing acetate from CO₂ acetate[49]. *Methanobrevibacter* is known for methanogenesis from CO₂ using hydrogen (Table 1, reaction (5)) or formate[50]. All *Methanobrevibacter* species grow well with hydrogen and CO₂[51], and several microbial electrosynthesis systems have reported presence of *Methanobrevibacter* [34,52,53]. The *Bacteroides* are gut and soil bacteria have shown sugar, fatty acid, and hydrocarbon degradation activity in other studies[54], suggesting that their role in the biotic reactors could be mainly related to the degradation of products and dead biomass material. However, some species of the *Bacteroides* genus are capable of fermentation[54] or even carbohydrate conversion to fatty acids combined with CO₂ capture[55].

Members of the *Rikenellaceae* family have been associated with the degradation of carbohydrates[56] and members of the *Rhodocyclaceae* family have been associated with acetate oxidation[57].

Based on the detected microorganism genera, *Peptococcaceae* species are suggested to be mainly responsible for acetogenesis in the systems of this study, the *Clostridium sensu stricto* 12 species will be responsible for the acetate elongation to *n*-butyrate and *n*-caproate, possibly together with *Bacteroides*. *Methanobrevibacter* is suggested to produce the observed methane and the *Rikenellaceae* and *Rhodocyclaceae* species are likely carbohydrate scavengers from e.g. decaying biomass. The higher relative abundance of *Clostridium sensu stricto* 12 species in the biotic VFAs reactor compared to the biotic CH₄ reactor (Table 2) corresponds with the observed higher volatile fatty acid productivities (Fig. 5). Furthermore, the higher relative abundance of *Methanobrevibacter* species in the biotic CH₄ reactor corresponds with the higher observed methane concentrations in the off gas of that reactor (Fig. 5). However, Cathode 2 shows similar relative abundance distributions for both biotic reactors (Table 2) despite the different measured net productivities, showing that productivities and functional groups can differ significantly between different locations at the cathode. Possibly the local hydrogen concentration differed over the different locations like in the biotic VFAs reactor (SI Fig. S7).

3.7. Outlook: Insights for electro-fermentation designs

The differences between the product spectra of the two biotic reactors show the importance of measuring local conditions and the effect of different local conditions on the microbial community. Despite the equal operation parameters and alternating flow-through regime, differences in local conditions could lead to different microbial activities. Although the thermodynamic calculations predicted an advantage for the methanogens (Table 1), other factors such as the elevated undissociated volatile fatty acid concentrations[58] could inhibit methanogenic organisms. In this study, even though the bulk pH was controlled at 5.8, hydrogen formation and its accompanied proton consumption, resulted in local higher pH values on the cathode surfaces. A local pH of 6.5 causes a decrease of 6% of the undissociated acetate concentration (compared to pH 5.8), which is beneficial for methanogenesis activity. The local hydrogen concentration is another factor that might influence the selection for either chain elongation or methanogenesis. The local hydrogen pressure in the methane forming reactor in this study was substantially lower than in the chain elongation reactor (Fig. 5C and SI Fig. S8A and B). The hydrogen pressure might have been detrimental for chain elongation microorganisms, since too low hydrogen pressure values have been shown to stimulate fatty acid oxidation rather than production[59]. Overall, monitoring local concentrations over time and investigating the effect of changing operating parameters on the local conditions is crucial. With this knowledge, the optimum operating

parameters can be selected and applied to steer the process towards either methanogenesis or chain elongation.

The results obtained in this work support the application potential of electro-fermentation processes like microbial electrosynthesis. First, the alternating flow-through regime allowed a start-up at high current density whilst maintaining hydrogen inside the porous cathode layers. Besides, this flow strategy decreased the power demand per kg hydrogen. The fast start-up at high current density was a crucial step forward on the previously reported need to focus on higher current density conditions [13,19,34,60]. However, further optimization is required to increase the electron recovery values into fatty acids. To increase the concentration of the desired products, it is recommended to focus on factors including energy efficiency, mass-transfer, biomass growth and selectivity of microbial conversions.

The energy efficiency of these systems is intrinsically related to the uptake of electrons from bacteria and their use to form added values compounds. Energy efficiencies decrease when a large fraction of the provided electrons (cathodic current) is lost in the form of hydrogen gas or used for competing processes (e.g. methanogenesis). The energy efficiency could be enhanced by the development of direct electron transfer mechanisms or application of intermittent current [61]. Based on the results of this study, it seems hydrogen availability cannot be limited at cathodes with low electric current since that might stop the chain elongation conversions. From the local measurements of hydrogen, it can be concluded that the hydrogen availability decreased over time (Fig. 6A and B). Therefore, with further development and maturation of the biofilm that grows on mediated electron transfer, it is expected that hydrogen becomes the limiting factor. To reduce dependency on hydrogen availability, the hydrogen supply could be slowly lowered over time by lowering the applied current. The lowering of the hydrogen availability could trigger development of direct electron uptake mechanisms in the microorganisms [62,63] and thus lower dependency on hydrogen as electron donor. An important note is that focussing on direct electron uptake as microbial energy source by reducing hydrogen also decreases the electron donor for suspended microorganisms. An alternative route for a more efficient electron transfer could be the external, electrochemical high-performance production of hydrogen [64], which can be supplied to the reactors [65]. This external introduction of the electron donor requires investigation since it would remove the need for bio-electrochemistry and thus also the reported issue of volatile fatty acid transport to the anode compartment.

To ensure sufficient mass-transfer in larger scale systems operating at high current density, it is recommended to measure local conditions with various large scale electrode designs. This allows to identify which electrode configuration gives the least mass-transfer limitations [6]. From a thermodynamic perspective, the acetate concentration is an important parameter as it determines the available energy for chain elongation. Therefore, monitoring acetate concentrations in the reactor, by means of e.g. an acetate probe [66], would give valuable real-time insights on the local conditions and the most favourable locations to achieve high biological activity. For further elucidation of important steering parameters and operating conditions, the microbial analysis should also be extended with e.g. activity or quantitative [67] analyses linked to local conditions.

The advantage of working with a mixed culture is the possibility of using selective pressure to enable the growth of the most robust microorganisms under a given set of operating conditions (e.g. salinity and pH). Given that mixed cultures are already present in waste streams, these streams could be used as an inflow source for bio-electrochemical CO₂ valorisation, without the need for aseptic methods. It should also be noted that, whilst the specific conditions of the three cathode layers and catholyte positions were identified, the spatial distribution of the microorganisms within the depth of the biofilm was not covered. Linking the spatial distribution of microbial groups on the cathode to the local conditions can give more insights on e.g. electron uptake mechanisms.

Finally, with the identification of the microbial community, operating conditions could be tested to favour the growth of the most biologically active bacteria. Once defined, these operating conditions could be applied for upscaling [15].

4. Conclusions

In this study, alternating flow-through was used to start-up bio-electrochemical systems at high current density. Alternating flow reduced the power input to 136 kWh per kg hydrogen. Start-up of microbial electrosynthesis systems with chain elongation was achieved within 10 days after start-up at constant applied current. After 60 days, local hydrogen concentrations between 100 and 600 μM were measured in the cathode layers, whilst 0.5–1 μM was measured in the bulk catholyte. The pH in the catholyte next to the cathodes were around 5.8–6.8. The alternating flow operation showed better mass-transfer, as both distribution of hydrogen to the cathode layers and also refreshing of possible “dead zones” were improved in the cathode chamber. Production of short and medium chain fatty acids was linked to presence of microorganisms classified as *Peptococcaceae* and *Clostridium sensu stricto* 12 species, whilst hydrogenotrophic methanogenesis was linked to *Methanobrevibacter*.

Declaration of Competing Interest

The authors declare that they have no known competing financial interests or personal relationships that could have appeared to influence the work reported in this paper.

Data availability

All raw data is deposited in the 4TU database with doi 10.4121/21583212.

Acknowledgements

The authors would like to thank Vinnie de Wilde and Michiel van den Broek for their assistance on the reactor setup. Thanks to the Wageningen EM center for facilitation of the SEM images. Thanks to Marten Gelderloos for his assistance on methane and 2-bromoethanesulfanoate measurements and the fruitful discussions. Thanks to João Pereira and Cees Buisman for manuscript revision.

Funding

This work was supported by Wageningen Institute for Environment and Climate research (WIMEK) and Chaincraft BV.

Appendix A. Supplementary data

Supplementary data to this article can be found online at <https://doi.org/10.1016/j.cej.2023.142599>.

References

- [1] B. Bian, S. Bajracharya, J. Xu, D. Pant, P.E. Saikaly, Microbial electrosynthesis from CO₂: Challenges, opportunities and perspectives in the context of circular bioeconomy, *Bioresource technology* 302 (2020), 122863.
- [2] M. Sharma, N. Aryal, P.M. Sarma, K. Vanbroekhoven, B. Lal, X.D. Benetton, D. Pant, Bioelectrocatalyzed reduction of acetic and butyric acids via direct electron transfer using a mixed culture of sulfate-reducers drives electrosynthesis of alcohols and acetone, *Chemical Communications* 49 (58) (2013) 6495–6497.
- [3] M. Yuan, M.J. Kummer, S.D. Minteer, Strategies for bioelectrochemical CO₂ reduction, *Chemistry–A, European Journal* 25 (63) (2019) 14258–14266.
- [4] I. Vassilev, P.A. Hernandez, P. Batlle-Vilanova, S. Freguia, J.O. Krömer, J.r. Keller, P. Ledezma, B. Virdis, Microbial electrosynthesis of isobutyric, butyric, caproic acids, and corresponding alcohols from carbon dioxide, *ACS Sustainable Chemistry & Engineering* 6 (7) (2018) 8485–8493.

- [5] M.C. van Eerten-Jansen, N.C. Jansen, C.M. Plugge, V. de Wilde, C.J. Buisman, A. ter Heijne, Analysis of the mechanisms of bioelectrochemical methane production by mixed cultures, *Journal of Chemical Technology & Biotechnology* 90 (5) (2015) 963–970.
- [6] L. Jourdin, T. Burdyny, Microbial electrosynthesis: where do we go from here? *Trends in Biotechnol.* 39 (4) (2021) 359–369.
- [7] L. Jourdin, S.M.T. Raes, C.J.N. Buisman, D.P.B.T.B. Strik, Critical Biofilm Growth throughout Unmodified Carbon Felts Allows Continuous Bioelectrochemical Chain Elongation from CO₂ up to Caproate at High Current Density, *Frontiers in Energy Research* 6 (2018), <https://doi.org/10.3389/fenrg.2018.00007>.
- [8] V. Flexer, L. Jourdin, Purposely Designed Hierarchical Porous Electrodes for High Rate Microbial Electrosynthesis of Acetate from Carbon Dioxide, *Acc Chem Res* 53 (2) (2020) 311–321, <https://doi.org/10.1021/acs.accounts.9b00523>.
- [9] R.A. Rozendal, H.V. Hamelers, C.J. Buisman, Effects of membrane cation transport on pH and microbial fuel cell performance, *Environmental science & technology* 40 (17) (2006) 5206–5211.
- [10] J.R. Kim, S. Cheng, S.-E. Oh, B.E. Logan, Power generation using different cation, anion, and ultrafiltration membranes in microbial fuel cells, *Environmental science & technology* 41 (3) (2007) 1004–1009.
- [11] H. Ooka, M.C. Figueiredo, M.T. Koper, Competition between hydrogen evolution and carbon dioxide reduction on copper electrodes in mildly acidic media, *Langmuir* 33 (37) (2017) 9307–9313.
- [12] A. De Lichtervelde, A. Ter Heijne, H. Hamelers, P. Biesheuvel, J. Dykstra, Theory of ion and electron transport coupled with biochemical conversions in an electroactive biofilm, *Phys. Rev. Appl.* 12 (1) (2019), 014018.
- [13] F. Kracke, A.B. Wong, K. Maegaard, J.S. Deutzmann, M.A. Hubert, C. Hahn, T. F. Jaramillo, A.M. Spormann, Robust and biocompatible catalysts for efficient hydrogen-driven microbial electrosynthesis, *Commun. Chem.* 2 (1) (2019) 45.
- [14] S.A. Patil, F. Harnisch, C. Koch, T. Hübschmann, I. Fetzer, A.A. Carmona-Martínez, S. Müller, U. Schröder, Electroactive mixed culture derived biofilms in microbial bioelectrochemical systems: the role of pH on biofilm formation, performance and composition, *Bioresource technology* 102 (20) (2011) 9683–9690.
- [15] I. Vassilev, F. Kracke, S. Freguia, J. Keller, J.O. Kromer, P. Ledezma, B. Virdis, Microbial electrosynthesis system with dual biocathode arrangement for simultaneous acetogenesis, solventogenesis and carbon chain elongation, *Chem Commun (Camb)* 55 (30) (2019) 4351–4354, <https://doi.org/10.1039/c9cc02088a>.
- [16] R.K. Brown, F. Harnisch, S. Wirth, H. Wahlandt, T. Dockhorn, N. Dichtl, U. Schröder, Evaluating the effects of scaling up on the performance of bioelectrochemical systems using a technical scale microbial electrolysis cell, *Bioresource Technology* 163 (2014) 206–213.
- [17] K. Katuri, M.L. Ferrer, M.C. Gutiérrez, R. Jiménez, F. Del Monte, D. Leech, Three-dimensional microchanneled electrodes in flow-through configuration for bioanode formation and current generation, *Energy & Environmental Science* 4 (10) (2011) 4201–4210.
- [18] L. Jourdin, T. Grieger, J. Monetti, V. Flexer, S. Freguia, Y. Lu, J. Chen, M. Romano, G.G. Wallace, J. Keller, High Acetic Acid Production Rate Obtained by Microbial Electrosynthesis from Carbon Dioxide, *Environ Sci Technol* 49 (22) (2015) 13566–13574, <https://doi.org/10.1021/acs.est.5b03821>.
- [19] E. Blanchet, F. Duquenne, Y. Raftari, L. Etcheverry, B. Erable, A. Bergel, Importance of the hydrogen route in up-scaling electrosynthesis for microbial CO₂ reduction, *Energy & Environmental Science* 8 (12) (2015) 3731–3744.
- [20] T.H. Sleutels, H.V. Hamelers, R.A. Rozendal, C.J. Buisman, Ion transport resistance in microbial electrolysis cells with anion and cation exchange membranes, *International Journal of Hydrogen Energy* 34 (9) (2009) 3612–3620.
- [21] S.M. de Smit, J.J.H. Langedijk, L.C.A. van Haalen, S.H. Lin, J.H. Bitter, D.P.B.T.B. Strik, Methodology for in-situ micro-sensor profiling of hydrogen, pH, ORP and electric potential throughout 3D porous cathodes of (bio)electrochemical systems, *ACS analytical chemistry* (2023), <https://doi.org/10.1021/acs.analchem.2c03121>.
- [22] S.M. de Smit, C.J. Buisman, J.H. Bitter, D.P. Strik, Cyclic Voltammetry is invasive on microbial electrosynthesis, *ChemElectroChem* 8 (17) (2021) 3384–3396.
- [23] A. Klindworth, E. Pruesse, T. Schweer, J. Peplies, C. Quast, M. Horn, F.O. Glöckner, Evaluation of general 16S ribosomal RNA gene PCR primers for classical and next-generation sequencing-based diversity studies, *Nucleic acids research* 41 (1) (2013) e1–e.
- [24] C. Quast, E. Pruesse, P. Yilmaz, J. Gerken, T. Schweer, P. Yarza, J. Peplies, F.O. Glöckner, The SILVA ribosomal RNA gene database project: improved data processing and web-based tools, *Nucleic acids research* 41(Database issue) (2013) D590–6. <https://doi.org/10.1093/nar/gks1219>.
- [25] R. Sander, Compilation of Henry's law constants (version 4.0) for water as solvent, *Atmos. Chem. Phys.* 15 (8) (2015) 4399–4981.
- [26] S.A. Patil, J.B. Arends, I. Vanwongterhem, J. Van Meerbergen, K. Guo, G.W. Tyson, K. Rabaey, Selective enrichment establishes a stable performing community for microbial electrosynthesis of acetate from CO₂, *Environmental science & technology* 49 (14) (2015) 8833–8843.
- [27] S. Bajracharya, R. Yuliasni, K. Vanbroekhoven, C.J. Buisman, D.P. Strik, D. Pant, Long-term operation of microbial electrosynthesis cell reducing CO₂ to multi-carbon chemicals with a mixed culture avoiding methanogenesis, *Bioelectrochemistry* 113 (2017) 26–34.
- [28] R. Ganigué, S. Puig, P. Batlle-Vilanova, M.D. Balaguer, J. Colprim, Microbial electrosynthesis of butyrate from carbon dioxide, *Chemical Communications* 51 (15) (2015) 3235–3238.
- [29] P. Batlle-Vilanova, R. Ganigué, S. Ramió-Pujol, L. Baneras, G. Jiménez, M. Hidalgo, M.D. Balaguer, J. Colprim, S. Puig, Microbial electrosynthesis of butyrate from carbon dioxide: production and extraction, *Bioelectrochemistry* 117 (2017) 57–64.
- [30] F. Wildenauer, K. Blotvogel, J. Winter, Effect of monensin and 2-bromoethane-sulfonic acid on fatty acid metabolism and methane production from cattle manure, *Applied Microbiology and Biotechnology* 19 (2) (1984) 125–130.
- [31] W. de Araújo Cavalcante, R.C. Leitão, T.A. Gehring, L.T. Angenent, S.T. Santaella, Anaerobic fermentation for n-caproic acid production: A review, *Process Biochemistry* 54 (2017) 106–119.
- [32] B. Schink, Energetics of syntrophic cooperation in methanogenic degradation, *Microbiology and molecular biology reviews* 61 (2) (1997) 262–280.
- [33] A. Lasia, Mechanism and kinetics of the hydrogen evolution reaction, *International journal of hydrogen energy*. 44(36). (2019). 19484–19518.
- [34] L. Jourdin, Y. Lu, V. Flexer, J. Keller, S. Freguia, Biologically induced hydrogen production drives high rate/high efficiency microbial electrosynthesis of acetate from carbon dioxide, *ChemElectroChem* 3 (4) (2016) 581–591.
- [35] S.M. Raes, L. Jourdin, C.J. Buisman, D.P. Strik, Bioelectrochemical Chain Elongation of Short-Chain Fatty Acids Creates Steering Opportunities for Selective Formation of n-Butyrate, n-Valerate or n-Caproate, *ChemistrySelect* 5 (29) (2020) 9127–9133.
- [36] Z. Lyu, N. Shao, T. Akinyemi, W.B. Whitman, Methanogenesis, *Current Biology* 28 (13) (2018) R727–R732.
- [37] D. Mayumi, J. Dolfig, S. Sakata, H. Maeda, Y. Miyagawa, M. Ikarashi, H. Tamaki, M. Takeuchi, C.H. Nakatsu, Y. Kamagata, Carbon dioxide concentration dictates alternative methanogenic pathways in oil reservoirs, *Nature communications* 4 (1) (2013) 1–6.
- [38] S. Schorberth, G. Gottschalk, Considerations on the energy metabolism of Clostridium kluyveri, *Archiv für Mikrobiologie* 65 (4) (1969) 318–328.
- [39] C. Fernández-Blanco, M.C. Veiga, C. Kennes, Efficient production of n-caproate from syngas by a co-culture of Clostridium acetium and Clostridium kluyveri, *Journal of environmental management* 302 (2022), 113992.
- [40] Y. Cui, K.-L. Yang, K. Zhou, Using co-culture to functionalize Clostridium fermentation, *Trends in Biotechnology* 39 (9) (2021) 914–926.
- [41] M.V. Reddy, S.V. Mohan, Y.-C. Chang, Medium-Chain Fatty Acids (MCFA) Production Through Anaerobic Fermentation Using Clostridium kluyveri: Effect of Ethanol and Acetate, *Applied Biochemistry and biotechnology* (2017) 1–12.
- [42] M. Köpke, C. Held, S. Hujer, H. Liesegang, A. Wiewer, A. Wollherr, A. Ehrenreich, W. Liebl, G. Gottschalk, P. Dürre, Clostridium ljungdahlii represents a microbial production platform based on syngas, *Proceedings of the National Academy of Sciences*. 107(29). (2010). 13087–13092.
- [43] J.K. Heffernan, K. Valgepea, R. de Souza Pinto, I. Lemgruber, M. Casini, R. Plan, S. D. Tappel, M. Simpson, L.K. Köpke, E.M. Nielsen, Enhancing CO₂-valorization using Clostridium autoethanogenum for sustainable fuel and chemicals production, *Frontiers in bioengineering and biotechnology* 8 (2020) 204.
- [44] Y. Shen, R. Brown, Z. Wen, Syngas fermentation of Clostridium carboxidivoran P7 in a hollow fiber membrane biofilm reactor: Evaluating the mass transfer coefficient and ethanol production performance, *Biochemical engineering journal* 85 (2014) 21–29.
- [45] Y. Zhu, S.T. Yang, Adaptation of Clostridium tyrobutyricum for Enhanced Tolerance to Butyric Acid in a Fibrous-Bed Bioreactor, *Biotechnology Progress* 19 (2) (2003) 365–372.
- [46] M. Atasoy, Z. Cetecioglu, Butyric acid dominant volatile fatty acids production: bio-augmentation of mixed culture fermentation by Clostridium tyrobutyricum, *Journal of Environmental Chemical Engineering* 8 (6) (2020), 104496.
- [47] Q. Wang, C.D. Wang, C.H. Li, J.G. Li, Q. Chen, Y.Z. Li, Clostridium luticellarii sp. nov., isolated from a mud cellar used for producing strong aromatic liquors, *Int J Syst Evol Microbiol* 65 (12) (2015) 4730–4733, <https://doi.org/10.1099/ijsem.0.000641>.
- [48] K.-R. Chatzipanagiotou, L. Jourdin, J.H. Bitter, D.P. Strik, Concentration-dependent effects of nickel doping on activated carbon biocathodes, *Catalysis Science & Technology* 12 (8) (2022) 2500–2518.
- [49] F. Liu, R. Conrad, Chemolithotrophic acetogenic H₂/CO₂ utilization in Italian rice field soil, *The ISME Journal* 5 (9) (2011) 1526–1539.
- [50] C. Vetriani, Archaea, Origin of, *Encyclopedia of Biodiversity: Second Edition*, Elsevier Inc. 2001. 218–226.
- [51] T.L. Miller, Methanobrevibacter, *Bergey's Manual of Systematics of Archaea and Bacteria* (2015) 1–14.
- [52] T. Gao, H. Zhang, X. Xu, J. Teng, Integrating microbial electrolysis cell based on electrochemical carbon dioxide reduction into anaerobic osmosis membrane reactor for biogas upgrading, *Water Research* 190 (2021), 116679.
- [53] M. Siegert, X.-F. Li, M.D. Yates, B.E. Logan, The presence of hydrogenotrophic methanogens in the inoculum improves methane gas production in microbial electrolysis cells, *Frontiers in microbiology* 5 (2015) 778.
- [54] H.N. Shah, The genus Bacteroides and related taxa, *The prokaryotes*, Springer, 1992, pp. 3593–3607.
- [55] M.A. Fischbach, J.L. Sonnenburg, Eating for two: how metabolism establishes interspecies interactions in the gut, *Cell host & microbe* 10 (4) (2011) 336–347.
- [56] D.W. Pitta, W.E. Pinchak, S.E. Dowd, J. Osterstock, V. Gontcharova, E. Youn, K. Dorton, I. Yoon, B.R. Min, J. Fulford, Rumen bacterial diversity dynamics associated with changing from bermudagrass hay to grazed winter wheat diets, *Microbial ecology* 59 (3) (2010) 511–522.
- [57] A. Oren, The family rhodocyclaceae, *The prokaryotes* 11 (2014) 975–998.
- [58] W. Zhang, K. Dai, X.-Y. Xia, H.-J. Wang, Y. Chen, Y.-Z. Lu, F. Zhang, R.J. Zeng, Free acetic acid as the key factor for the inhibition of hydrogenotrophic methanogenesis in mesophilic mixed culture fermentation, *Bioresource technology* 264 (2018) 17–23.
- [59] S. Ge, J.G. Usack, C.M. Spirito, L.T. Angenent, Long-term n-caproic acid production from yeast-fermentation beer in an anaerobic bioreactor with continuous product extraction, *Environmental science & technology* 49 (13) (2015) 8012–8021.

- [60] D.C. Calvo, A. Ontiveros-Valencia, R. Krajmalnik-Brown, C.I. Torres, B. E. Rittmann, Carboxylates and alcohols production in an autotrophic hydrogen-based membrane biofilm reactor, *Biotechnology and bioengineering* 118 (6) (2021) 2338–2347.
- [61] A. Ter Heijne, M. Pereira, J. Pereira, T. Sleutels, Electron storage in electroactive biofilms, *Trends in Biotechnology* 39 (1) (2021) 34–42.
- [62] D.J. Walker, K.P. Nevin, D.E. Holmes, A.-E. Rotaru, J.E. Ward, T.L. Woodard, J. Zhu, T. Ueki, S.S. Nonnenmann, M.J. McInerney, Syntrophus conductive pili demonstrate that common hydrogen-donating syntrophs can have a direct electron transfer option, *The ISME journal* 14 (3) (2020) 837–846.
- [63] A.-E. Rotaru, P.M. Shrestha, F. Liu, M. Shrestha, D. Shrestha, M. Embree, K. Zengler, C. Wardman, K.P. Nevin, D.R. Lovley, A new model for electron flow during anaerobic digestion: direct interspecies electron transfer to *Methanosaeta* for the reduction of carbon dioxide to methane, *Energy & Environmental Science* 7 (1) (2014) 408–415.
- [64] A. Hodges, A.L. Hoang, G. Tsekouras, K. Wagner, C.-Y. Lee, G.F. Swiegers, G. Wallace, A high-performance capillary-fed electrolysis cell promises more cost-competitive renewable hydrogen, *Nature communications* 13 (1) (2022) 1–11.
- [65] F.C. Baleeiro, S. Kleinstueber, H. Sträuber, Hydrogen as a co-electron donor for chain elongation with complex communities, *Frontiers in bioengineering and biotechnology* 9 (2021), 650631.
- [66] E. Atci, J.T. Babauta, S.T. Sultana, H. Beyenal, Microbiosensor for the detection of acetate in electrode-respiring biofilms, *Biosensors and Bioelectronics* 81 (2016) 517–523.
- [67] S.D. Molenaar, T. Sleutels, J. Pereira, M. Iorio, C. Borsje, J.A. Zamudio, F. Fabregat-Santiago, C.J. Buisman, A. Ter Heijne, In situ biofilm quantification in bioelectrochemical systems by using optical coherence tomography, *ChemSusChem* 11 (13) (2018) 2171–2178.